Emerging Contaminants 11 (2025) 100532

Contents lists available at ScienceDirect

Emerging Contaminants

journal homepage: www.keaipublishing.com/en/journals/emerging-contaminants

Efficient photocatalytic degradation of metoprolol using activated carbon supported NiFe-layered double hydroxides (NiFe-LDH/C) under solar-driven simulation

Raphael N. Biata [a,*], Wendy Mabhulusa [a], Lethula E. Mofokeng [b], Rudzani Ratshiedana [a], Tshimangadzo S. Munonde [a], Edward N. Nxumalo [a,**]

[a] Institute for Nanotechnology and Water Sustainability, College of Science, Engineering and Technology, University of South Africa, Roodepoort, 1709, South Africa
[b] Department of Chemistry, Faculty of Natural and Agricultural Sciences, University of Pretoria, Private Bag X20, Hatfield, Pretoria, South Africa

ARTICLE INFO

Article history:
Received 12 December 2024
Received in revised form
29 April 2025
Accepted 6 June 2025
Available online 19 June 2025

Keywords:
NiFe-LDH/C
β-blockers
Metoprolol
Photodegradation
UPLC-MS

ABSTRACT

The efficient photocatalytic degradation of pharmaceuticals in wastewater is critically important for environmental protection. The synthesis and characterization of NiFe-LDH/C for the photocatalytic degradation of selected β-blockers, specifically metoprolol, under UV light conditions were investigated in this study. The study aimed to explore the potential of NiFe-LDH/C as a catalyst for the degradation of metoprolol, a commonly used pharmaceutical compound in the treatment of chronic diseases such as high blood pressure and chest pains, which is frequently detected in wastewater. The selection of NiFe-LDH/C was driven by the need for materials with high photocatalytic activity, the ability to generate reactive oxygen species and enhance charge separation, and stability under solar light. Activated carbon was employed as a support to increase the surface area and improve the dispersion of the LDH particles, thereby enhancing overall photocatalytic efficiency. The results showed that NiFe-LDH/C exhibited excellent photocatalytic activity in degrading metoprolol under both UV and sunlight-mediated conditions, with degradation efficiencies of over 89 %. Furthermore, the characterization of the NiFe-LDH/C catalyst revealed its stability and recyclability, making it a promising candidate for the efficient removal of pharmaceutical compounds from wastewater through photocatalytic degradation. The characterization results showed that the NiFe-LDH/C exhibited a high degree of crystallinity and a well-defined layered structure. The photocatalytic experiments demonstrated that the NiFe-LDH/C was effective in degrading metoprolol and ultra-performance liquid chromatography-mass spectrometry (UPLC-MS) was used to elucidate the degradation products of metoprolol in water.

1. Introduction

Water contamination caused by β-blockers is a growing environmental health hazard [1–3]. β-blockers, a class of pharmaceuticals primarily used to manage cardiovascular conditions such as hypertension and heart arrhythmias, have been detected in water bodies worldwide [4–6]. The main sources of β-blockers contamination in water systems include effluent from wastewater treatment plants [7,8], runoff from agricultural lands where livestock are treated with these medications [9,10], and improper disposal of unused medications [11,12]. The presence of β-blockers in water bodies can adversely affect aquatic organisms, including disruptions in endocrine systems, changes in behaviour, and reproductive abnormalities [2–4,13]. β-blockers (e.g., atenolol, metoprolol, propranolol) are widely detected in wastewater due to incomplete metabolism and limited removal in conventional treatment plants. Recent studies highlight their persistence and potential ecological risks, including endocrine disruption and cardiotoxicity in aquatic organisms [14]. Advanced oxidation processes (AOPs), particularly photocatalysis, have gained

* Corresponding author.
** Corresponding author.
E-mail addresses: biatanr@unisa.ac.za (R.N. Biata), nxumaen@unisa.ac.za (E.N. Nxumalo).
Peer review under the responsibility of KeAi Communications Co., Ltd.

https://doi.org/10.1016/j.emcon.2025.100532

attention for their ability to degrade these pharmaceuticals efficiently [15]. Metoprolol is a commonly used β-blocker for the treatment of cardiovascular illnesses [16,17] and is also often found in water environments [2,3,18]. Metoprolol removal effectiveness in WWTPs varies significantly based on the factors of WWTP design and operation. [19,20]. Additionally, there are concerns about the potential for bioaccumulation of β-blockers in aquatic food chains, leading to further ecological impacts. Among these adverse consequences include decreased testosterone levels, endocrine system disturbance, and sexual dysfunction. [21]. Constantly using β-blockers in quantities higher than the daily maximum of μg-ng/dm^3 has negative health effects. [22,23]. Therefore, coming up with efficient ways to eradicate these erratic pollutants is a huge area of research. Techniques for removal, such as adsorption [24], photodegradation [2,3,25], membrane filtration [26] among others, have been given serious consideration in the fight against these resistant β-blockers. Therefore, it is crucial to identify novel catalytic materials with promising activity, high stability, and good durability [27,28].

Layered double hydroxides (LDHs), sometimes referred to as hydrated metal-like compounds, are a type of layered composite metal hydroxide made up of exchangeable anions placed in between the layers and divalent and trivalent metal cations [31–35]. $[M^{3+}_xM^{2+}_{1-x}(OH)^2]^x + [An^-]_{x/n}{\cdot}mH_2O]$ is the description of the particular structure of LDH, where M^{2+} and M^{3+} stand for divalent metal cations (such as Zn^{2+}, Ni^{2+}, and so on) and trivalent metal cations (such as Al^{3+}) respectively [36]. LDHs are highly valued as exceptional photocatalytic materials because of their exceptional qualities, which include uniform distribution of metal cations, excellent interlayer anion exchangeability, biocompatibility, and chemical stability [37,38]. Furthermore, by carefully choosing and managing the right metal cations and interlayer anions, LDHs provide adjustable reactive site locations and band gaps, improving the effectiveness of visible light use [39]. These characteristics give LDHs exceptional organic pollutant adsorption capacities. Moreover, the formation of heterostructures of LDHs with metals, hydroxides, other semiconductors, or salts allows the achievement of particular band gap values. [39]. These characteristics have inspired scientists to develop LDH-based photocatalytic materials. For example, [29] used an electrostatic assembly approach to create a new three-dimensional layered NiFe-LDH/C photocatalyst [36]. When exposed to visible light, this catalyst demonstrated an ideal H2 production 6.23 times greater than that of pure CdS [36]. However, LDHs have the following drawbacks: quick photo-induced charge carrier recombination, weak reduction ability, limited recycling ability following the photocatalytic reaction, and strong adsorption capacity [33,40,41]. Their overall conversion efficiency is constrained by these issues. Additionally, their photocatalytic activities are further impeded by inadequate functional group loading [42]. Researchers are actively investigating various modification techniques to develop high-performance LDH-based composites for photocatalytic applications. Carbon-based materials, such as carbon nanotubes [43], graphene oxide [44], and annealed nanodiamonds [45], have typically been utilized in recent years to support metal-based catalysts. Activated carbon (C) is the most commonly utilized carbon material in wastewater treatment as a carbon support for metal-based catalysts due to its remarkable adsorptive capacity and catalytic activity.

Our objective was to utilize the distinct characteristics of cutting-edge materials such as C and LDHs to create a new, highly effective NiFe-LDH/C catalyst that would aid in the photocatalytic degradation of metoprolol in the presence of UV light. Various characterization instruments utilized to explore the chemical and physical characteristics of the NiFe-LDH/C composites. In addition, the catalyst dose was taken into consideration when determining the catalytic activity of NiFe-LDH/C composites. More significantly, the UHPLC-MS technique was used to determine the metoprolol breakdown process and the by-products potentially produced.

2. Materials and methods

2.1. Materials

All chemicals used were of analytical reagent grade, and ultrapure water was used throughout the experiments. Urea (ACE, South Africa), $Fe(NO_3)_2{\cdot}9H_2O$, $Ni(NO_3)_2{\cdot}6H_2O$, ethanol, methanol, formic acid, ascorbic acid were all supplied by Sigma Aldrich (South Africa) and ammonia (25 %) were obtained from Merck (Johannesburg, South Africa). A 1.00 g metoprolol/L stock solution was made by dissolving metoprolol tartrate, which was acquired from Sigma-Aldrich (USA), in methanol.

2.2. Synthesis of NiFe-LDH and NiFe-LDH/C

With some typical modification, NiFe-LDH/C was produced using the prior hydrothermal technique [46]. In 80 mL of deionized (DI) water, 1.33 g of $Fe(NO_3)_2.9H_2O$ and 3.90 g of $Ni(NO_3)_2.6H_2O$ were dissolved, and the mixture was agitated for 15 min. Subsequently, an activated carbon suspension was introduced to this solution, which was made by sonicating 0.5 g of activated carbon in 10 mL of DI H_2O for 5 min. For 30 min, the suspension was swirled. After 30 min of stirring and adding 1.94 g urea, the mixture was moved to a stainless-steel autoclave lined with Teflon and heated to 150 °C for 21 h. The autoclave was then allowed to cool to ambient temperature, and the product was cleaned using a centrifuge. The finished product was then pulverized into a fine powder after being dried for the entire night at 100 °C in an oven. The synthesis procedure described above was used to synthesize NiFe-LDH; however, activated carbon solution was not added.

2.3. Photocatalytic performance evaluation

Metoprolol's degradation under simulated solar light irradiation was used to gauge the photocatalytic activities of the synthesized composites. A 300 W xenon lamp solar simulator (HAL-350) fitted with $\lambda \geq 300$ nm cut-off filters was used as the light source. A typical run involved adding 80 mg of photocatalysts to a beaker that contained 100.0 mL of pollutant aqueous solution (20.0 mg L^{-1}, without adjusting pH). To reach adsorption-desorption equilibrium before irradiation, the suspension was stirred in the dark for 30 min. Then, at predetermined intervals, 3.0 mL suspension samples were removed and filtered using 0.22 μm PES syringe filters (ANPEL, China) in preparation for additional analysis. The average values with standard deviations were presented after the batch experiments were carried out in triplicate.

2.4. Electrochemical investigation

The electrochemical examinations were performed using a Biologic (Biologic Science Instruments GmbH, Germany) three-electrode system equipped with a glassy carbon electrode ((GCE), diameter: 3 mm; A = 0.071 cm^2), working electrode (WE), Pt electrode as the counter electrode, and a silver-silver chloride (Ag/AgCl) as the reference electrode containing the saturated NaCl solution (~3 M). The standard electrode modification involved

ultrasonically dispersing 20 mg of NiFe-LDH/C in 5 mL of ethanol, creating a homogenous suspension. 5 μL of this suspension were then drop cast onto a well-polished GCE and baked at 80 °C. A NiFe-LDH-modified electrode was made for comparison using the same process as previously described. The WE were cleaned using alumina slurries (1, 0.3, and 0.05 μm) and rinsed with deionized water before drop-casting. The WE were then sonicated in DI H_2O and ethanol for 15 min to remove the particles of alumina slurries on the surface of the electrode and the electrode was dried before the modification. The cyclic voltametric (CV) test was carried out in an N_2-purged with 5 mM of Ferri/ferrocyanide in 0.1 M KCl used as an electrolyte at 100 mV s^{-1} between −1 V and +1 V vs Ag/AgCl. The electrochemical impendency spectroscopy (EIS) experiments were carried out in the same solution at a fixed potential window (0.421 and 0.29 V vs Ag/AgCl) for NiFe-LDH and NiFe-LDH/C, respectively.

3. Results and discussion

3.1. Chemical composition analysis

3.1.1. Fourier Transform Infrared Spectroscopy (FTIR) analysis of C, NiFe-LDH and NiFe-LDH/C

The FTIR spectra (Fig. 1) were used to analyze the chemical bonds associated with the molecular interactions of C, NiFe-LDH, and NiFe-LDH/C. The expansive bands around 3434 and 1618 cm^{-1} are linked to the hydroxyl (OH) group and the flexural vibration of hydroxyls in the layer [47]. The shoulder band observed near 3240 cm^{-1} indicates the possible remaining amine groups from the NH_4^+ produced during urea breakdown in the hydrothermal synthesis process [46]. The band at 1383 cm^{-1} is attributed to the anti-symmetric stretching vibration of the intercalating CO_3^{2-} anion, which is a direct consequence of urea breakdown during hydrothermal synthesis [43]. The stretching band observed at 2153 cm^{-1} is primarily due to the C-O vibrations of the CO_3^{2-} anions and the activated carbon backbone, highlighting their significant role in this interaction [43,44]. The lattice vibrations of Ni-O, Fe-O, and Ni-O-Fe in the brucite layer of the LDH play a crucial role in generating the broad bands at approximately 656 and 497 cm^{-1}, highlighting their significance in the material's properties [45].

3.2. X-ray Diffraction (XRD) analysis of C, NiFe-LDH and NiFe-LDH/C

The XRD pattern of the NiFe-LDH/C and NiFe-LDH sample as prepared is displayed in Fig. 2. The standard diffraction patterns of the NiFe-Layered Double Hydroxide (LDH) structures, as referenced in JCPDS card No. 40–0215 and source [46], closely correspond to the typical characteristic peaks associated with NiFe-LDH. These peaks were observed at angles of 11.88°, 22.44°, 34.25°, 39.33°, 46.59°, 59.53°, and 61.10°. The corresponding diffraction peaks for these angles are attributed to the following planes: (003), (006), (012), (015), (018), (110), and (113), respectively. The (003) and (006) peaks are indicative of the layered structure typical of LDHs. The presence of these specific peaks suggests that the LDH maintains its characteristic brucite-like structure, where metal hydroxide layers alternate with interlayer anions or water molecules. The undifferentiated, abrupt peak shape could show that the produced NiFe-LDH had good crystallization, due to fewer defects (such as stacking faults or amorphous regions) present. This reduces peak broadening in XRD and results in sharper diffraction peaks (Fig. 2) [48]. While the NiFe-LDH/C did not show sharper peaks, which might be attributed to the method of synthesis and any post-synthesis processes (such as calcination or drying) may also have an impact on the material's crystallinity. For example, synthesis carried out hydrothermally or at low temperature may result in less crystallinity than synthesis carried out using high-temperature treatment. Furthermore, the large diffraction peaks at 25.8° and 40.7° are indicative of the amorphous activated carbon's (002) and (101) diffraction planes.

3.3. Particle morphology analysis of C, NiFe-LDH and NiFe-LDH/C

3.3.1. Field emission scanning electron microscope (FE-SEM) and EDS and energy dispersive X-ray spectroscopy (EDS)

To study the morphologies and structures of the NiFe-LDH and NiFe-LDH/C, FE-SEM was used. The NiFe-LDH nanoclusters have layered structures, as shown in Fig. 3a and NiFe-LDH/C in Fig. 3b. The EDS spectra confirmed the presence of Ni, Fe, O and C in Fig. 3c for NiFe-LDH/C. The aluminium detected in the materials arises from the possible sample contact with the specimen stubs. This emphasizes the necessity for meticulous handling to guarantee

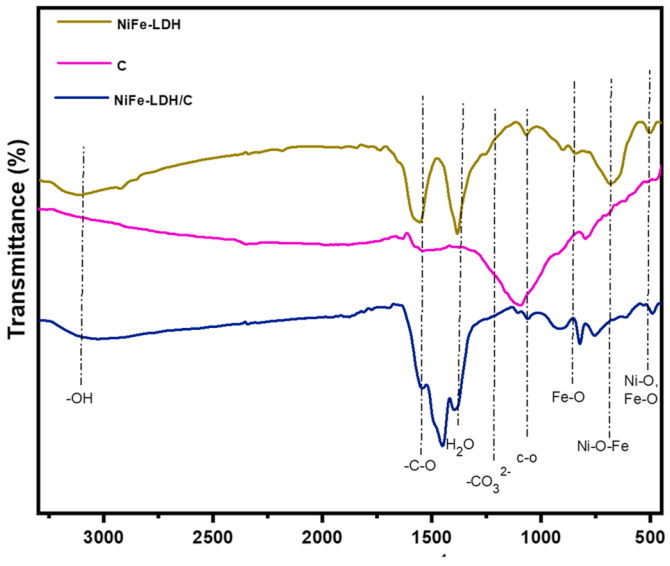

Fig. 1. FTIR spectra for (a) NiFe-LDH, (b) C, (c) NiFe-LDH/C.

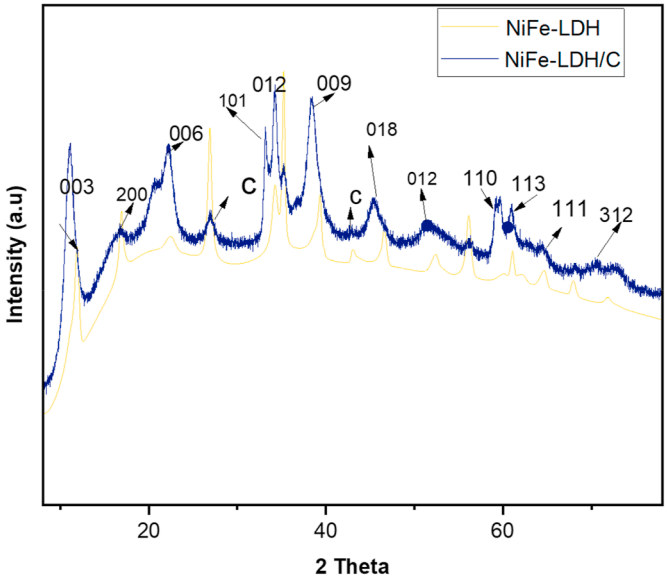

Fig. 2. XRD pattern of NiFe-LDH/C and NiFe-LDH.

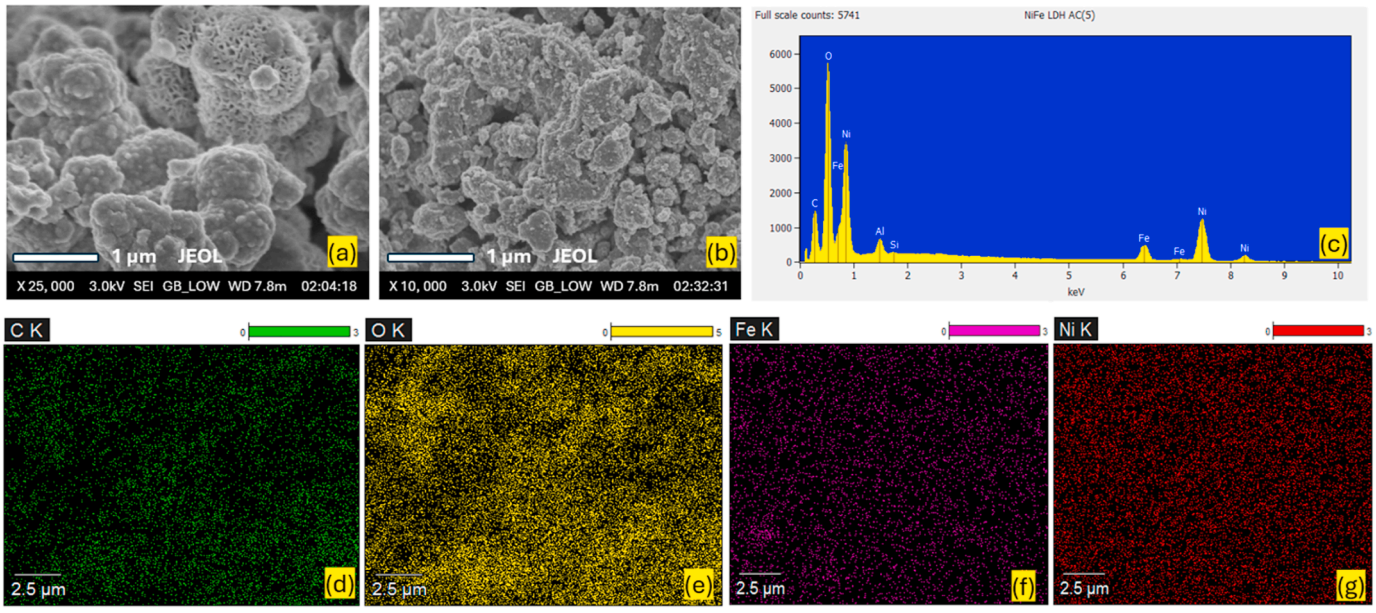

Fig. 3. FE-SEM images for surface morphology of (a) NiFe-LDH, (b) NiFe-LDH/C, (c) EDS spectra of NiFe-LDH/C and (d)–(g) mapping images of NiFe-LDH/C.

accurate results. The elements C, O, Fe and Ni were evenly distributed on the catalyst surface, as shown by the EDS mapping images of the NiFe-LDH/C (Fig. 3(d,e,f and g)). The presence of increased oxygen as observed in SEM mapping can play a dual role. It can enhance photocatalytic activity by improving charge separation and facilitating the generation of reactive species.

3.3.2. *High-resolution transmission electron microscopy/selected area electron diffraction (HR-TEM/SAED)*

Activated carbon sheets support the NiFe-LDH/C multilayers, as seen in the TEM image in Fig. 4a. The SAED pattern of the NiFe-LDH/C (Fig. 4b) shows distinct polyatomic bright spots, which correspond to specific lattice planes of the NiFe-LDH structure. The intensity of these bright spots indicates a well-defined crystalline structure, affirming the successful synthesis of the NiFe-LDH/C. The presence of these sharp spots suggests a high degree of crystallinity, which is crucial for photocatalytic applications [49]. The FE-SEM images clearly show that adding activated carbon sheets reduced the aggregation and stacking of the NiFe-LDH/C layers, resulting in greater exposure. The presence of diffraction rings indicates that although the material is mainly crystalline, the activated carbon provides sufficient surface area, which can enhance the adsorption of metoprolol.

3.4. *Brunauer–Emmett–Teller (BET) surface area analysis of C, NiFe-LDH and NiFe-LDH/C*

The N_2 adsorption-desorption isotherms recorded at 77 K were used to characterize the pores for NiFe-LDH and NiFe-LDH/C (Fig. 5). The specific surface area of NiFe-LDH/C was 176.3 m^2/g, significantly more than that of NiFe-LDH, which had a specific surface area of 84.8 m^2/g. The addition of activated carbon, which is known to have a large surface area (198.1 m^2/g), is responsible for the significant increase in surface area [50].

As can be shown in Table 2, NiFe-LDH/C exhibited higher average pore size and total pore volume than NiFe-LDH (see Table 1). NiFe-LDH and NiFe-LDH/C are also shown in the inset graph of Fig. 5. According to the International Union of Pure and Applied Chemistry's (IUPAC) classification, the presence of mesoporous material was suggested by the type IV isotherm with an H3-type hysteresis loop.

3.5. *Optical response of C, NiFe-LDH and NiFe-LDH/C*

The quantity of catalyst used in photocatalytic degradation is one of the variables affecting the process efficiency. Thus, the effects of different catalyst dosages (20–80 mg) on the photocatalytic

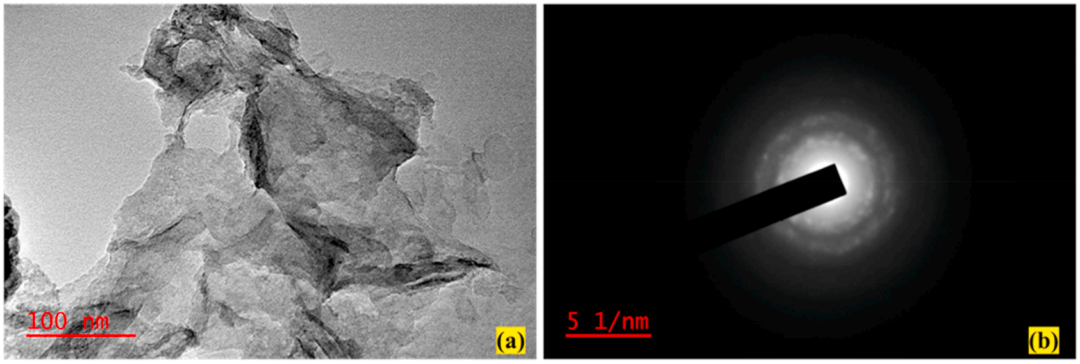

Fig. 4. TEM image of (a) NiFe-LDH/C and (b) SAED pattern of NiFe-LDH/C.

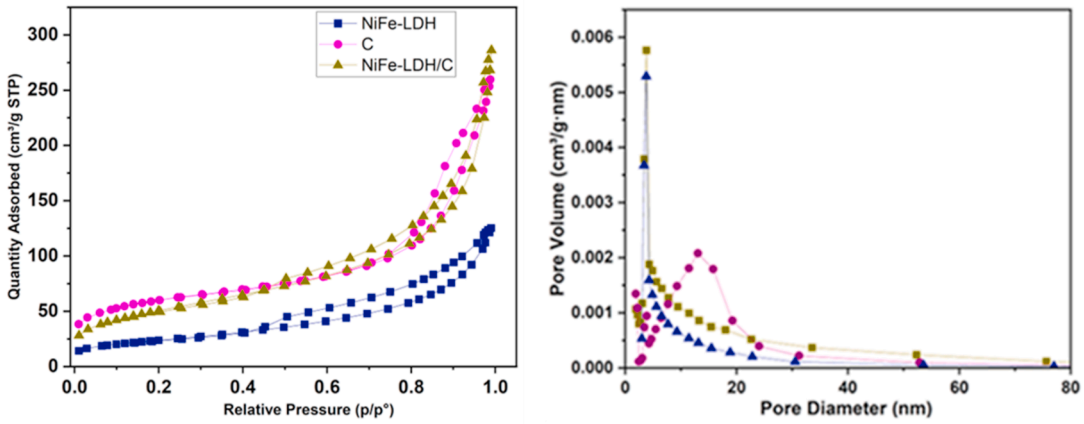

Fig. 5. Nitrogen adsorption-desorption isotherms of C, NiFe-LDH and NiFe-LDH/C and the corresponding pore-size distribution calculated by the BJH method.

Table 1
Physicochemical properties of metoprolol β-blockers.

Chemical structure	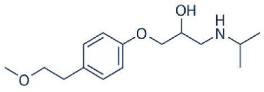
Chemical formula	$C_{15}H_{25}NO_3$
Molecular weight (g/mol)	267.36 g/mol
Solubility in water (0.402 mg/mL at 25 °C).	0.402 mg/mL
λ_{max} (nm)	275
Therapeutic group	β-blockers

Table 2
BET properties of C, NiFe-LDH and NiFe-LDH/C.

Surface properties	C	NiFe-LDH	NiFe-LDH/C	Surface properties
BET surface area (m^2/g)	198.12	84.83	176.27	BET surface area (m^2/g)
Average pore size (nm)	6.16	6.30	6.93	Average pore size (nm)
Total pore volume (cm^3/g)	0.32	0.15	0.29	Total pore volume (cm^3/g)

activity were investigated (Fig. 5a). Through an increase in catalyst dosage from 20 mg to 80 mg, the efficiency of pollutant degradation was improved. High catalyst dosages can result in excessive light scattering, which may hinder photocatalytic degradation [51]. Thus, 80 mg was determined to be the ideal catalyst dosage for further experimental work. Using different catalysts of C, NiFe-LDH and NiFe-LDH/C degraded 52 %, 71 %, and 89 % of pollutants with 24 % from photolysis, respectively, as shown in Fig. 5b. It is clear that NiFe-LDH/C exhibited the highest pollutant degrading efficiency; hence, it was the most suitable catalyst for the subsequent experiment's tests. As shown in section 3.6, its high photocatalytic activity can enhanced the visible light harvesting, decreased charge transfer resistance, rapid electron migration, and suppressed recombination of photogenerated electron-hole pairs [52]. As seen in Fig. 5c, the Langmuir-Hinshelwood model was fitted to the data to fully evaluate the samples' photocatalytic degradation rates. At low initial pollutant concentration (C_0), the model is essentially a pseudo-first-order kinetic reaction with the formula:

$$\ln(C_0 / C_t) = kt \quad (1)$$

Where k is the reaction rate constant and C_t and C_0 are the dye concentrations at times t = t and t = 0 respectively. The estimated sample rate constant values are shown in Fig. 5c. It was shown that NiFe-LDH/C composite enhanced the photocatalytic activity. This implies that the interfaces between AC and NiFe-LDH may enhance the formation process, reactive species separation, and charge carrier transfer, all of which may result in a higher degradation efficiency of pollutants.

3.6. Electrochemical behaviour of the prepared NiFe-LDH and NiFe-LDH/C

CV was used to investigate the electron mobility in electrochemical reactions using NiFe-LDH and NiFe-LDH/C as photocatalysts. When the C dopant was applied to NiFe-LDH, the CV in Fig. 6A demonstrate an increase in the observed anodic peak current. The enhanced electron mobility is responsible for the observed anodic peak current augmentation. Furthermore, the rapid electron transfer on the photocatalyst surface is indicated by the anodic peak shift of NiFe-LDH/C to a more negative potential. The broad peak for the anodic and cathodic scan was observed at 0.28 V vs Ag/AgCl (anodic peak) and 0.16 V vs Ag/AgCl (cathodic peak) for NiFe-LDH/C and 0.43 V vs Ag/AgCl (anodic peak) and 0.07 V vs Ag/AgCl (cathodic peak) LDH. To verify the analytical data of NiFe-LDH/C and LDH obtained from CV, EIS was employed as shown in Fig. 6B**.** NiFe-LDH/C (0.5 kΩ) has a smaller semicircle than LDH (4.5 kΩ), which indicates a reduced electron charge transfer resistance/polarization resistance (Rct/Rp). A tiny arc is therefore favored for the materials' possible usage in

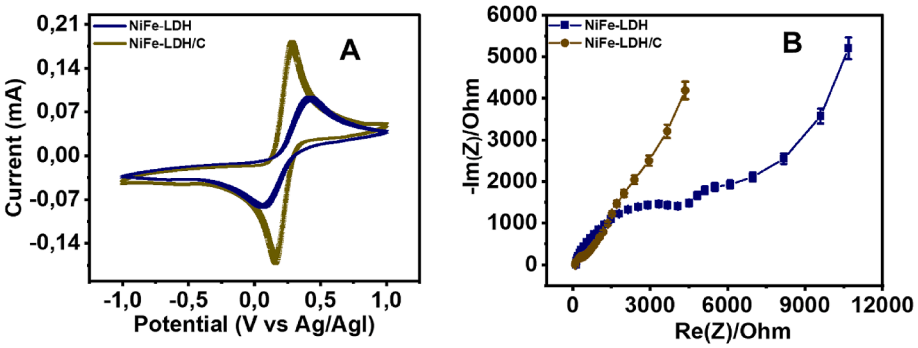

Fig. 6. CV (A), and Nyquist plot (B) of NiFe-LDH and NiFe-LDH/C in an N_2-purged, 5 mM of Ferri/ferrocyanide at 100 mV s^{-1} plotted with error bars for the electrodes (NiFe-LDH and NiFe-LDH/C), n = 4 for each data point, standard error represented by error bars.

photocatalysis since it mimics the material's surface's decreased electron transfer resistance, which leads to efficient charge separation between electrons and holes. Doping the NiFe-LDH with C enhanced its electron charge transfer, which in turn enhanced photocatalytic performance, as seen in Fig. 6B. The synergistic effects of C facilitate better charge carrier mobility, increase the number of active sites, enhance light absorption, and improve the overall stability of the composite. Thus, the observed results agree with the data obtained from the CV results.

3.7. Degradation pathway

The UPLC-MS analysis (Figure S1 (a-b) was performed to elucidate the degradation products of metoprolol in water. The peak intensity of pure metoprolol was significantly reduced concerning the degraded metoprolol after 180 min, signifying a concentration reduction of metoprolol in water. Several metoprolol metabolites with the mass-to-charge (*m/z*) ratio of 225, 211, 209, 207, 179, 177, 166, and 138 *m/z* were identified from the mass spectra and the degradation pathway is shown in Fig. 7. The initial step is initiated by the electron transfer to the amine group, followed by the abstraction of proton in the solution causing demethylation to form **P1** (1-[4-(2-methoxyethyl)phenoxy]-3-[(propan-2-yl)amino]propan-2-ol) with *m/z* of 225 [53,54]A further attack on the adjacent carbon to methoxy group led to the emanation of **P2** (1-amino-3-[4-(2-hydroxyethyl)phenoxy]propan-2-ol) and the reduction of P2 led to a C=O bond as shown **P3** ([4-(3-amino-2-hydroxypropoxy) phenyl]acetaldehyde) [55]Whereas, **P3** (209 *m/z*) and **P4** ((2*E*)-3-[4-(2-methoxyethyl)phenoxy]prop-2-en-1-amine) products were produced due to the elimination of water and C=O and C=C bonds were formed. The loss of the methoxy group due to hydroxyl radical attack led to the formation of **P5** ((4-{[(1*E*)-3-aminoprop-1-en-1-yl]oxy}phenyl)methanol) and the -OH reduction yielded **P6** (4-{[(1*E*)-3-aminoprop-1-en-1-yl]oxy}benzaldehyde) having the carbonyl group. The P7 (4-(2-methoxyethyl)phenol) was formed as the result of aryl ether C-O bond cleavage to give rise to P7. Furthermore, the elimination of the methoxy group on **P7** led to the emergence of **P8** (4-(2-hydroxyethyl)phenol), where the subsequent radical attack on the P8 can lead to even smaller by-products and the production of CO_2 and water [56].

3.8. Possible photocatalytic mechanism

The degradation of metoprolol using NiFe-LDH/C comprises of the adsorption of metoprolol on the surface of the NiFe-LDH/C catalyst and is followed by catalytic degradation reactions after the irradiated light with the same or higher energy than the band gap of the photocatalyst which will cause the generation of photo-excited electrons (e^-) and holes (h^+). The NiFe-LDH/C has a band gap of 2.37 eV, which can be photoexcited using visible light irradiation, as shown in Fig. 8. After visible light irradiation, the electrons (e^-) in the valence band (VB) are excited and migrate into the conduction band (CB) of NiFe-LDH, leaving the holes (h^+) behind on the VB. However, the rapid recombination of photo-excited e^-/h^+ pairs may occur as a result of a narrow band gap of NiFe-LDH, subsequently leading to minimal photocatalytic degradation efficiency. To overcome the recombination of photoexcited e^-/h^+ pairs, activated carbon (C) was utilized as a support material for NiFe-LDH and as an electron acceptor for the photoexcited e^- in the CB of NiFe LDH, which is transferred to the CB of C. This process improved the photoexcited charge separation and minimized the high rate of photoexcited e^-/h^+ pairs, thus enhancing the photocatalytic efficiency of metoprolol. Typically, the photoexcited e^- in the CB of NiFe-LDH is unable to react with the adsorbed O_2 in the surface of the photocatalyst since NiFe-LDH has a weaker CB edge potential (−0.31V vs NHE) than −0.33V vs NHE of O_2/O_2^- [57]. However, the photoexcited e^- in the CB of C can reduce the adsorbed O_2 to yield superoxide radicals (O_2^-) due to more negative CB edge potential (−1.14V vs NHE) of C as compared to −0.33V vs NHE reduction potential of O_2/O_2^- [58]. On the other hand, the VB holes (h^+) in the NiFe-LDH have a more positive VB band potential of 2.55V vs NHE than 2.27V vs NHE of •OH/-OH. Hence, the h^+ can oxidize water and hydroxyl species to generate hydroxyl radicals (•OH). Conversely, C cannot oxidize water in the VB of C due to a lower oxidation potential (1.56V vs NHE) than 2.27V vs NHE of •OH/-OH [58]. The main reactive radicals which were •OH and O_2^- contributed significantly to the degradation of metoprolol into smaller compounds such as water, carbon dioxide, and other by-products. Due to the synergetic properties of NiFe-LDH/C, the material can be regarded as superior for the eradication and degradation of baneful pollutants in the environment. The probable reaction mechanism is outlined as follows [59].

$$\text{NiFe-LDH} + h\nu \rightarrow \text{NiFe-LDH}\,(e^-_{CB} + h^+_{VB}) \quad (2)$$

$$\text{NiFe-LDH}\,(e^-_{CB} + h^+_{VB}) + C \rightarrow \text{NiFe-LDH}\,(h^+_{VB}) + C\,(e^-_{CB}) \quad (3)$$

$$C\,(e^-_{CB}) + O_2 \rightarrow O_2^{-\bullet} \quad (4)$$

$$h^+_{(VB)} + H_2O \rightarrow \bullet OH + H^+ \quad (5)$$

$$\text{Metoprolol} + O_2^{-\bullet} + \bullet OH \rightarrow H_2O + CO_2 + \text{by-products} \quad (6)$$

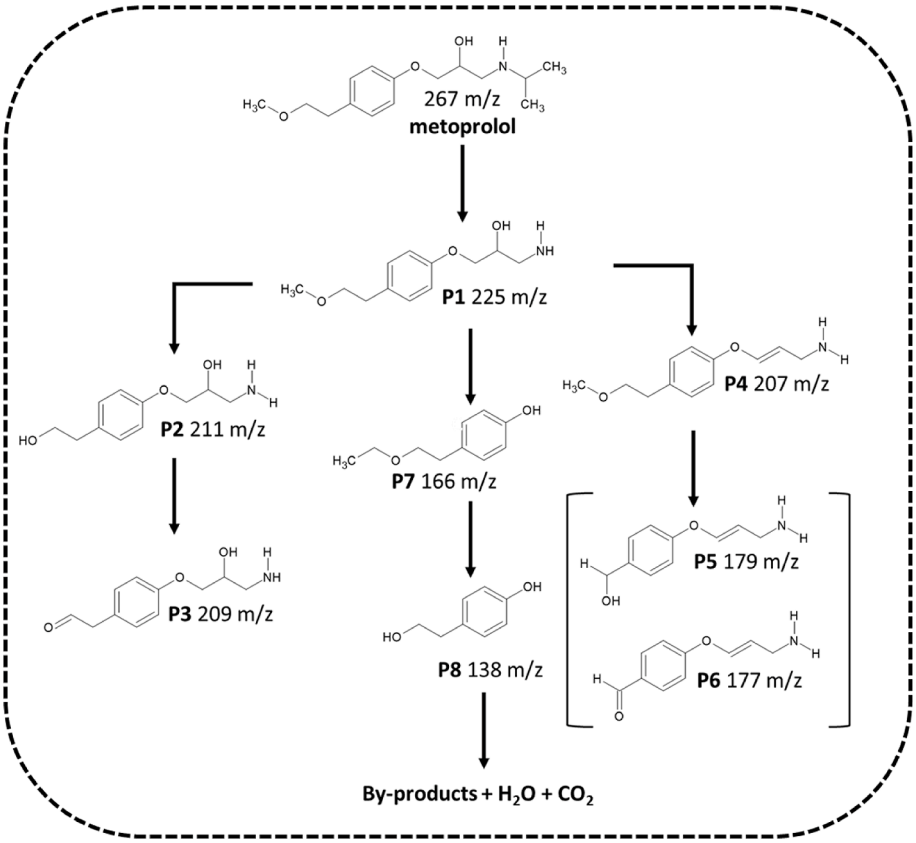

Fig. 7. The proposed photocatalytic degradation pathway for metoprolol using NiFe-LDH/C.

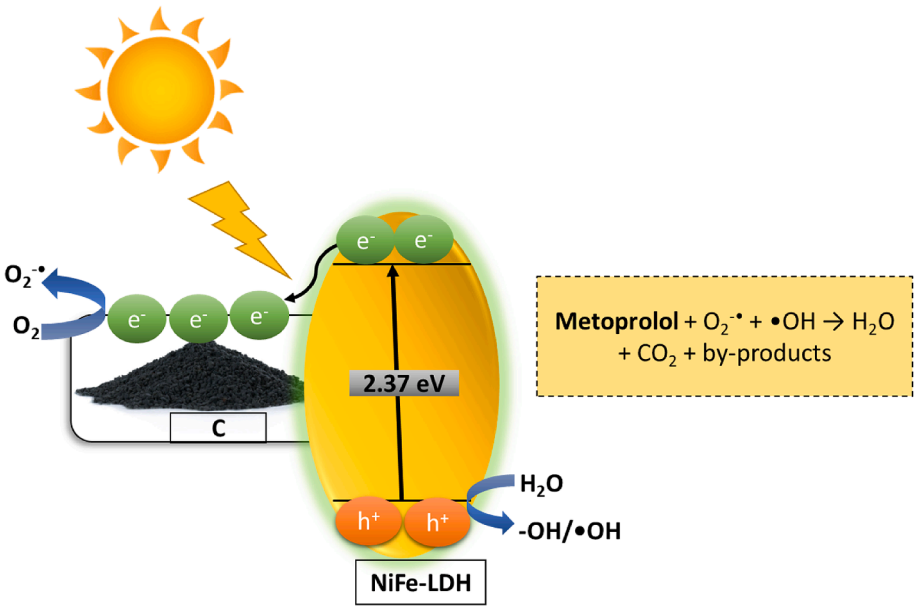

Fig. 8. Possible degradation mechanism for metoprolol in the presence of NiFe-LDH/C photocatalyst.

3.9. Toxicity evaluation

The toxicity of the parent compound and degradation products were estimated using the Quantitative structure–activity relationship models (QSAR models) and the results are shown in Table 3.The QSAR model works by analysing the relationship between the chemical structures and their potential effects on living organisms, in this case the non-target organism *Daphnia magna*. Due to the highly lipophilic nature of metoprolol [60], as the parent compound, it has shown to be more toxic than its metabolites (P1-P8) reported in Table 3. However, compared to other metabolites, the results in Table 3 show that P4, 5 and 6 are

Table 3
QSAR model toxicity assessments of the identified degradation products.

Degradation products	Toxicity Assessment
P1 (1-[4-(2-methoxyethyl)phenoxy]-3-[(propan-2-yl)amino]propan-2-ol)	342.98
P2 (1-amino-3-[4-(2-hydroxyethyl)phenoxy]propan-2-ol)	136.25
P3 ([4-(3-amino-2-hydroxypropoxy)phenyl]acetaldehyde)	155.31
P4 ((2E)-3-[4-(2-methoxyethyl)phenoxy]prop-2-en-1-amine)	281.03
P5 ((4-{[(1E)-3-aminoprop-1-en-1-yl]oxy}phenyl)methanol)	249.38
P6 (4-{[(1E)-3-aminoprop-1-en-1-yl]oxy}benzaldehyde)	260.19
P7 (4-(2-methoxyethyl)phenol)	92.47
P8 (4-(2-hydroxyethyl)phenol)	87.24

Table 4
Comparison of proposed catalyst with existing systems.

Catalyst Type	Advantages	Limitations	Degradation Efficiency (for β-blockers)	References
Fe_3O_4@ TiO_2-P25	High UV activity, stable	Limited visible-light response	~60–80 % (UV, 2h)	[66]
Ag-TiO_2	Enhanced visible absorption, antibacterial	Costly, potential metal leaching	~85–90 % (visible, 2h)	[67]
g-C_3N_4-based	Low-cost, tunable bandgap	Fast charge recombination	~70–75 % (visible, 3h)	[68]
Perovskites ($BiFeO_3$)	Ferroelectric, broad light absorption	Complex synthesis	~90–95 % (solar, 2h)	[69]
$BiVO_4$/g-C_3N_4	Efficient charge separation, solar-driven	Stability issues in long-term use	~95 % (visible, 1.5h)	[70]
NiFe-LDH/C	Enhanced visible-light absorption and stability	long-term stability under continuous flow conditions	89 % (visible, 3h)	This work

Table 5
Comparison of NiFe-LDH catalysts with other LDH catalyst used for degradation of organic pollutants.

Catalyst	Method of synthesis	Pollutant	Reusability	R (%)	Ref
FeAl-LDH	Hydrothermal	Bisphenol A	–	93.0 %	[71]
ZnCo–LDH@CeO_2	Hydrothermal	phenol	5 cycles	99 %	[72]
NiFeLa-LDH	Co-precipitation	Tetracycline	–	90.0 %	[73]
CoFe-LDH	Co-precipitation	Ciprofloxacin	2 cycles	76 %	[74]
NiFe-LDH	Hydrothermal	Metoprolol	5 cycles	71 %	This work
NiFe-LDH/C	Hydrothermal	Metoprolol	5 cycles	89 %	This work

closely toxic to the parent compound. This can be ascribed to presence of the double bond (C=C) in P4, 5 and 6 that is more reactive than an OH group (alcohol) in other metabolites, as the pi bond in the double bond is weaker and more susceptible to attack by environmental reagents, leading to addition reactions that activate the more toxic nature of these metabolites [61–63]. It is noteworthy that P7 and P8 were found to be less toxic than the parent metoprolol compound, which is supported by the literature [63–65].

Table 4 compares the proposed NiFe-LDH/C catalyst with existing systems for β-blocker degradation. While conventional TiO_2 exhibits limited visible-light activity and Ag-TiO_2 suffers from metal leaching, NiFe-LDH/C offers enhanced visible-light absorption and stability due to its layered structure and carbon support. Compared to g-C_3N_4 (charge recombination issues) and perovskites (complex synthesis), NiFe-LDH/C demonstrates competitive efficiency (>85 %) with simpler preparation.

Table 5 compares NiFe-LDH with other LDH catalysts (e.g., CoFe-LDH, FeAl-LDH) for organic pollutant degradation. NiFe-LDH demonstrates superior redox activity and visible-light response due to its Fe^{3+}/Fe^{2+} and Ni^{2+}/Ni^{3+} couples, achieving >89 % pollutant removal.

4. Conclusion

In this study, we successfully synthesized and characterized activated carbon-supported NiFe-LDH (NiFe-LDH/C) as an efficient photocatalyst for the degradation of metoprolol under simulated solar irradiation. The material's structural, morphological, and optical properties were confirmed through various analytical techniques, demonstrating a well-distributed NiFe-LDH on the activated carbon surface. The photocatalytic performance of NiFe-LDH/C was evaluated, revealing a significant enhancement in metoprolol degradation (over 89 %) compared to pure NiFe-LDH and activated carbon alone. The results showed that NiFe-LDH/C exhibited high photocatalytic activity, attributed to the synergistic effects between NiFe-LDH and the activated carbon support. These effects include increased surface area, improved light absorption, and enhanced charge separation efficiency, which collectively contribute to the effective degradation of metoprolol. Additionally, the study confirmed that the material's photocatalytic efficiency is influenced by factors such as catalyst dosage, and the presence of oxidants, highlighting the potential for optimizing reaction conditions. Furthermore, the NiFe-LDH/C composite displayed excellent reusability, maintaining a high photocatalytic efficiency over 5 cycles with minimal loss in performance. Overall, the NiFe-LDH/C composite demonstrates considerable potential as a sustainable and efficient photocatalyst for the removal of pharmaceutical contaminants from water, particularly under solar irradiation. For further application, the photocatalytic degradation process could be employed in wastewater treatment plants or decentralized systems to remove pharmaceutical pollutants from water sources, helping mitigate the environmental impact of pharmaceutical residues. Thus, NiFe LDH/C catalyst could be applied in the remediation of other organic contaminants, expanding its utility beyond just pharmaceutical degradation to a wide range of industrial effluents containing pesticides, dyes, and other harmful pollutants. One area for

improvement is the long-term stability and reusability of NiFe-LDH/C. Photocatalysts can often suffer from deactivation over multiple cycles, especially under harsh environmental conditions. Optimizing the catalyst's stability and regeneration capabilities would be crucial for making it more viable for real-world, long-term applications.

CRediT authorship contribution statement

Raphael N. Biata: Writing – original draft, Visualization, Validation, Methodology, Investigation, Formal analysis, Data curation, Conceptualization. **Wendy Mabhulusa:** Writing – review & editing, Writing – original draft, Formal analysis, Data curation. **Lethula E. Mofokeng:** Writing – review & editing, Methodology, Conceptualization. **Rudzani Ratshiedana:** Investigation, Data curation. **Tshimangadzo S. Munonde:** Writing – review & editing, Supervision, Investigation, Conceptualization. **Edward N. Nxumalo:** Writing – review & editing, Resources, Project administration, Funding acquisition, Conceptualization.

Declaration of competing interest

The authors declare the following financial interests/personal relationships which may be considered as potential competing interests: Edward Nxumalo reports financial support was provided by Sasol Ltd. If there are other authors, they declare that they have no known competing financial interests or personal relationships that could have appeared to influence the work reported in this paper.

Acknowledgements

The authors gratefully acknowledge the financial support from SASOL (Grant No: SASOL791027) and the National Research Foundation. Special thanks are also extended to the Institute for Nanotechnology and Water Sustainability at the University of South Africa for their additional funding and for providing laboratory space to facilitate this research.

Appendix A. Supplementary data

Supplementary data to this article can be found online at https://doi.org/10.1016/j.emcon.2025.100532.

References

[1] R.K. Mishra, S.S. Mentha, Y. Misra, N. Dwivedi, Emerging pollutants of severe environmental concern in water and wastewater: a comprehensive review on current developments and future research, Water-Energy Nexus 6 (2023) 74–95.
[2] P.P. Mashile, T.S. Munonde, P.N. Nomngongo, Occurrence and adsorptive removal of sulfonamides and $β$-blockers in African and Asian water matrices: a comprehensive review, Environ. Adv. (2023) 100435.
[3] N.J. Waleng, S.K. Selahle, A. Mpupa, Y. Zhang, P.N. Nomngongo, Development of magnetic solid phase micro-extraction (MSPE) method for the extraction and preconcentration of the selected $β$-Blockers in the environmental wastewaters, Chem. Afr. (2024) 1–17.
[4] Ł. Wołowiec, et al., Beta-blockers in cardiac arrhythmias–Clinical pharmacologist's point of view, Front. Pharmacol. 13 (2023) 1043714.
[5] A. Bathinapatla, S. Kanchi, R. Chokkareddy, R.P. Puthalapattu, M.R. Kumar, Recent trends in the electrochemical sensors on β-and calcium channel blockers for hypertension and angina pectoris: a comprehensive review, Microchem. J. 192 (2023) 108930.
[6] H. Wang, S. Wang, S. Wang, L. Fu, L. Zhang, Efficient metal-organic framework adsorbents for removal of harmful heavy metal Pb (II) from solution: activation energy and interaction mechanism, J. Environ. Chem. Eng. 11 (2) (2023) 109335.
[7] J. Liu, et al., Occurrence and removal rate of typical pharmaceuticals and personal care products (PPCPs) in an urban wastewater treatment plant in beijing, China, Chemosphere 339 (2023) 139644.
[8] S. Choi, et al., Occurrence, removal, and prioritization of organic micropollutants in four full-scale wastewater treatment plants in Korea, Chemosphere 361 (2024) 142460.
[9] D. Ram\'irez-Morales, et al., Pharmaceuticals, hazard and ecotoxicity in surface and wastewater in a tropical dairy production area in Latin America, Chemosphere 346 (2024) 140443.
[10] B. Yurdakok-Dikmen, N. Tresnakova, A. Filazi, C. Faggio, Biological wastewater treatment systems for the biodegradation and detoxification of pharmaceuticals, in: Pharmaceuticals in Aquatic Environments, CRC Press, 2024, pp. 65–86.
[11] S.M. Benny, S.D. Gupta, S.P. Ismail, D. Francis, Pharmaceutical pollution of water bodies: sources, impacts, and mitigation, Handb. Water Pollut. (2024) 371–416.
[12] U.L. Usman, S. Banerjee, N.B. Singh, Emerging micropollutants in aquatic environment, toxicity effects and their removal techniques, in: Nanotechnology to Monitor, Remedy, and Prevent Pollution, Elsevier, 2024, pp. 373–409.
[13] H.M. Shihomatsu, E.A.J. Martins, M.E.B. Cotrim, D.T. Lebre, M.A.F. Pires, others, Occurrence of $β$-blocker and antihypertensive in water supply reservoir, Guarapiranga dam, São Paulo, SP, Brazil, in: XXXIV CONGRESSO INTERAMERICANO DE INGENIERIA SANIATARIA Y AMBIENTAL, 2014b, Monterrey, 2015, pp. 1–6.
[14] A. Kujawska, U. Kiełkowska, A. Atisha, E. Yanful, W. Kujawski, Comparative analysis of separation methods used for the elimination of pharmaceuticals and personal care products (PPCPs) from water–A critical review, Sep. Purif. Technol. 290 (2022) 120797.
[15] P.K. Pandis, et al., Key points of advanced oxidation processes (AOPs) for wastewater, organic pollutants and pharmaceutical waste treatment: a mini review, ChemEngineering 6 (1) (2022) 8.
[16] N. Johri, P.S. Matreja, A. Maurya, S. Varshney, others, Role of $β$-blockers in preventing heart failure and major adverse cardiac events post myocardial infarction, Curr. Cardiol. Rev. 19 (4) (2023) 24–31.
[17] R.A. Maheshwari, et al., Metoprolol and bisoprolol in coronary artery disease: an observational prospective cross-sectional Study, J. Young Pharm. 16 (1) (2024) 42–49.
[18] J.W. Kingsbury, K.J. Hartman, The potential impacts of statins and beta-blockers on West Virginia ichthyofauna, Water 15 (20) (2023) 3536.
[19] L. Molnarova, T. Halesova, D. Tomesova, M. Vaclavikova, Z. Bosakova, Monitoring pharmaceuticals and personal care products in healthcare effluent wastewater samples and the effectiveness of drug removal in wastewater treatment plants using the UHPLC-MS/MS method, Molecules 29 (7) (2024) 1480.
[20] X. Yang, R. Zou, K. Tang, H.R. Andersen, I. Angelidaki, Y. Zhang, Degradation of metoprolol from wastewater in a bio-electro-fenton system, Sci. Total Environ. 771 (2021) 145385.
[21] M.T. Wheeler, et al., Effect of beta-blocker therapy on the response to mavacamten in patients with symptomatic obstructive hypertrophic cardiomyopathy, Eur. J. Heart Fail. 25 (2) (2023) 260–270.
[22] H.-B. Lee, K. Sarafin, T.E. Peart, Determination of $β$-blockers and $β$2-agonists in sewage by solid-phase extraction and liquid chromatography–tandem mass spectrometry, J. Chromatogr. A 1148 (2) (2007) 158–167.
[23] A. Küster, et al., Environmental risk assessment of human pharmaceuticals in the European Union: a case study with the $β$-blocker atenolol, Integrated Environ. Assess. Manag. 6 (S1) (2010) 514–523.
[24] G.Z. Kyzas, A. Koltsakidou, S.G. Nanaki, D.N. Bikiaris, D.A. Lambropoulou, Removal of beta-blockers from aqueous media by adsorption onto graphene oxide, Sci. Total Environ. 537 (2015) 411–420.
[25] J. Wang, et al., Photochemical fate of $β$-blocker pindolol in riverine and its downstream coastal waters, Sci. Total Environ. 927 (2024) 172236.
[26] J.M. Thomas, C.T. Aravindakumar, U.K. Aravind, Removal of beta blockers using polyelectrolyte monolayered membrane and its antifouling performance, J. Ind. Eng. Chem. 87 (2020) 222–233.
[27] S. Gupta, R. Fernandes, R. Patel, M. Spreitzer, N. Patel, A review of cobalt-basedcatalysts for sustainable energy and environmental applications, Appl. Catal. Gen. 661 (2023) 119254.
[28] F. Shi, et al., Emerging catalytic materials for practical lithium-sulfur batteries, J. Energy Chem. 76 (2023) 127–145.
[29] X. Gao, et al., Construction of black g-C3N4/loofah/chitosan hydrogel as an efficient solar evaporator for desalination coupled with antibiotic degradation, Sep. Purif. Technol. 355 (2025) 129615.
[31] A. Sethurajaperumal, V. Ravichandran, A. Banerjee, A. Manohar, E. Varrla, Two-dimensional layered nanosheets: structure and unique properties, in: Fundamentals and Properties of Multifunctional Nanomaterials, Elsevier, 2021, pp. 465–497.
[32] D.-G. Jeung, T.-H. Kim, J.-M. Oh, Homogeneous incorporation of gallium into layered double hydroxide lattice for potential radiodiagnostics: proof-of-concept, Nanomaterials 11 (1) (2020) 44.
[33] J. Zheng, et al., Tourmaline/ZnAL-LDH nanocomposite based photocatalytic system for efficient degradation of mixed pollutant wastewater, Sep. Purif. Technol. 345 (2024) 127306.
[34] R. Pelalak, A. Hassani, Z. Heidari, M. Zhou, State-of-the-art recent applications of layered double hydroxides (LDHs) material in Fenton-based oxidation processes for water and wastewater treatment, Chem. Eng. J. (2023) 145511.
[35] A. Farhan, et al., Progress in layered double hydroxides (LDHs): Synthesis and application in adsorption, catalysis and photoreduction, Sci. Total Environ.

(2023) 169160.
[36] E.M. Seftel, et al., LDH and TiO2/LDH-type nanocomposite systems: a systematic study on structural characteristics, Microporous Mesoporous Mater. 203 (2015) 208–215.
[37] T. Hu, et al., Layered double hydroxide-based nanomaterials for biomedical applications, Chem. Soc. Rev. 51 (14) (2022) 6126–6176.
[38] G. Chakraborty, R. Padmashree, A. Prasad, Recent advancement of surface modification techniques of 2-D nanomaterials, Mater. Sci. Eng. B 297 (2023) 116817.
[39] A.A. Khan, M. Tahir, N. Khan, LDH-based nanomaterials for photocatalytic applications: a comprehensive review on the role of bi/trivalent cations, anions, morphology, defect engineering, memory effect, and heterojunction formation, J. Energy Chem. 84 (2023) 242–276.
[40] X. Sun, et al., Flower-like spherical ZnCdS/Bi2WO6/ZnAl-LDH with dual type II heterostructure as a photocatalyst for efficient photocatalytic degradation and hydrogen production, J. Phys. Chem. Solid. 183 (2023) 111650.
[41] X. Gan, D. Lei, Plasmonic-metal/2D-semiconductor hybrids for photodetection and photocatalysis in energy-related and environmental processes, Coord. Chem. Rev. 469 (2022) 214665.
[42] A. Sherryna, M. Tahir, Recent developments in layered double hydroxide structures with their role in promoting photocatalytic hydrogen production: a comprehensive review, Int. J. Energy Res. 46 (3) (2022) 2093–2140.
[43] H. Gao, X. Han, R. Wang, K. Zhu, R. Han, Adsorption and catalytic degradation of bisphenol A and p-chlorophenol by magnetic carbon nanotubes, Environ. Res. 231 (2023) 116314.
[44] C. Huang, et al., Peroxymonosulfate activation by graphene oxide-supported 3D-MoS2/FeCo2O4 sponge for highly efficient organic pollutants degradation, Environ. Pollut. 325 (2023) 121391.
[45] F. Miao, C. Cheng, W. Ren, H. Zhang, S. Wang, X. Duan, Dual nonradical catalytic pathways mediated by nanodiamond-derived sp2/sp3 hybrids for sustainable peracetic acid activation and water decontamination, Environ. Sci. \& Technol. 58 (19) (2024) 8554–8564.
[46] T.S. Munonde, H. Zheng, P.N. Nomngongo, Ultrasonic exfoliation of NiFe LDH/CB nanosheets for enhanced oxygen evolution catalysis, Ultrason. Sonochem. 59 (2019) 104716.
[47] X. Liu, J. Shi, X. Bai, W. Wu, Ultrasound-excited hydrogen radical from NiFe layered double hydroxide for preparation of ultrafine supported Ru nanocatalysts in hydrogen storage of N-ethylcarbazole, Ultrason. Sonochem. 81 (2021) 105840, https://doi.org/10.1016/j.ultsonch.2021.105840.
[48] X. Zhao, et al., Surfactant-modified flowerlike layered double hydroxide-coated magnetic nanoparticles for preconcentration of phthalate esters from environmental water samples, J. Chromatogr. A 1414 (2015) 22–30, https://doi.org/10.1016/j.chroma.2015.07.105.
[49] L. Muñoz-Fernandez, A. Sierra-Fernández, G. Flores-Carrasco, O. Milošević, M. E. Rabanal, Solvothermal synthesis of Ag/ZnO micro/nanostructures with different precursors for advanced photocatalytic applications, Adv. Powder Technol. 28 (1) (2017) 83–92.
[50] K.M. Dimpe, L. Nyaba, C. Magoda, J.C. Ngila, P.N. Nomngongo, Synthesis, modification, characterization and application of AC@Fe2O3@MnO2 composite for ultrasound assisted dispersive solid phase microextraction of refractory metals in environmental samples, Chem. Eng. J. 308 (Jan. 2017) 169–176, https://doi.org/10.1016/j.cej.2016.09.079.
[51] W. Xu, et al., Synergy mechanism for TiO2/activated carbon composite material: photocatalytic degradation of methylene blue solution, Can. J. Chem. Eng. 100 (2) (2022) 276–290.
[52] Z. Chen, et al., Simultaneously enhanced photon absorption and charge transport on a distorted graphitic carbon nitride toward visible light photocatalytic activity, Appl. Catal. B Environ. 242 (2019) 40–50.
[53] Y. Li, J. Sun, S.-P. Sun, Comparison of metoprolol degradation by FeIII-NTA modified Fenton-like reaction in the absence and presence of manganese: efficiency and intermediates, Chem. Eng. J. 313 (2017) 769–776.
[54] Y. Chen, et al., Oxidation of $β$-blockers by birnessite: kinetics, mechanism and effect of metal ions, Chemosphere 194 (2018) 588–594.
[55] B. Abramović, S. Kler, D. Šojić, M. Laušević, T. Radović, D. Vione, Photocatalytic degradation of metoprolol tartrate in suspensions of two TiO2-based photocatalysts with different surface area. Identification of intermediates and proposal of degradation pathways, J. Hazard. Mater. 198 (2011) 123–132.
[56] A. Pinedo, M. López, E. Leyva, B. Zermeño, B. Serrano, E. Moctezuma, Photocatalytic decomposition of metoprolol and its intermediate organic reaction products: kinetics and degradation pathway, Int. J. Chem. React. Eng. 14 (3) (2016) 809–820.
[57] J. Yan, X. Zhang, W. Zheng, L.Y.S. Lee, Interface engineering of a 2D-C3N4/NiFe-LDH heterostructure for highly efficient photocatalytic hydrogen evolution, ACS Appl. Mater. \& Interfaces 13 (21) (2021) 24723–24733.
[58] J. Hemalatha, M. Senthil, D. Madhan, A.M. Al-Mohaimeed, W.A. Al-onazi, Fabrication of NiFe2O4 nanoparticles loaded on activated carbon as novel composites for high efficient ultra violet-light photocatalysis for degradation of aqueous organic pollutants, Diam. Relat. Mater. 144 (2024) 110995.
[59] T.S. Munonde, N. Madima, R. Ratshiedana, P.N. Nomngongo, L.E. Mofokeng, R. S. Dima, Synergistic adsorption-photocatalytic remediation of methylene blue dye from textile industry wastewater over NiFe LDH supported on tyre-ash derived activated carbon, Appl. Surf. Sci. 679 (2025) 161205.
[60] M.M. Khalid, M.A. Galuska, R.J. Hamilton, Beta-Blocker Toxicity, 2017.
[61] D. Ravelli, S. Protti, M. Fagnoni, Carbon–carbon bond forming reactions via photogenerated intermediates, Chem. Rev. 116 (17) (2016) 9850–9913.
[62] L. Chen, et al., Solar-light-activated periodate for degradation and detoxification of highly toxic 6PPD-quinone at environmental levels, Nat. Water 2 (5) (2024) 453–463.
[63] S.-Q. Yang, R.-Q. Ye, Y.-H. Cui, Z.-Q. Liu, K. Sun, Y.-Z. Yu, Transformation of metoprolol in UV/PDS process: role and mechanisms of degradation and polymerization, J. Hazard. Mater. 472 (2024) 134498.
[64] J. Yao, Y. Sun, Y. Tang, Y. Zhang, W. Wu, J. Sun, Atmospheric oxidation of 4-(2-methoxyethyl) phenol initiated by OH radical in the presence of O2 and NOx: a mechanistic and kinetic study, Int. J. Quantum Chem. 121 (13) (2021) e26650.
[65] I. Kalaiselvan, S.M. Dicson, P.D. Kasi, Olive oil and its phenolic constituent tyrosol attenuates dioxin-induced toxicity in peripheral blood mononuclear cells via an antioxidant-dependent mechanism, Nat. Prod. Res. 29 (22) (2015) 2129–2132.
[66] J. López Gallego, A. Rey Barroso, E. Viñuelas Zah\'inos, P.M. Álvarez Peña, Preparation of a New Green Magnetic Fe3O4@ TiO2-P25 Photocatalyst for Solar Advanced Oxidation Processes in Water, 2023.
[67] M.Y. Naz, S. Shukrullah, H.N. Bhatti, others, Growth of Ag, TiO 2 and AgTiO 2 nanoparticles through liquid-Plasma interaction for bacterial and wastewater treatment, Pakistan J. Agric. Sci. 61 (3) (2024).
[68] S. Soni, S. Teli, P. Teli, S. Agarwal, Empowering sustainability: charting the seven years of progress in g-C_3N_4 based materials and their crucial role in building a greener future, Sustain. Chem. Pharm. 41 (2024) 101693.
[69] P.K. Harijan, S. Singh, P. Singh, P.K. Yadav, D.G. Ji, Structural, morphological, and optical investigation of PbTiO3 doped BiFeO3 nanoparticles derived from sol-gel method, Eng. Res. Express 7 (2) (2025) 025002.
[70] A. Riapanitra, T. Setyaningtyas, and G. H. Haryadinaru, "Photodegradation of methylene blue dye using $BiVO_4$/g-C_3N_4 composites under visible light irradiation," J. Kim. Sains dan Apl., vol. 27, no. 8, pp. 363–370.
[71] Q. Ye, et al., Enhancing peroxymonosulfate activation of Fe-Al layered double hydroxide by dissolved organic matter: performance and mechanism, Water Res. 185 (2020) 116246.
[72] Q. Gao, Y. Cui, S. Wang, B. Liu, C. Liu, Enhanced photocatalytic activation of peroxymonosulfate by CeO2 incorporated ZnCo–layered double hydroxide toward organic pollutants removal, Sep. Purif. Technol. 263 (2021) 118413.
[73] R. Wang, S. Su, X. Ren, W. Guo, Polyoxometalate intercalated La-doped NiFe-LDH for efficient removal of tetracycline via peroxymonosulfate activation, Sep. Purif. Technol. 274 (2021) 119113.
[74] Z. Yang, et al., Facile synthesis of cobalt-iron layered double hydroxides nanosheets for direct activation of peroxymonosulfate (PMS) during degradation of fluoroquinolones antibiotics, J. Clean. Prod. 310 (2021) 127584.